Inorganic Chemistry

pubs.acs.org/IC Article

Microwave-Assisted Synthesis of Tris-Anderson Polyoxometalates for Facile CO_2 Cycloaddition

Wei-Dong Yu,* Yin Zhang, Yu-Yang Han, Bin Li, Sai Shao, Le-Ping Zhang, Hong-Ke Xie, and Jun Yan*

Cite This: *Inorg. Chem.* 2021, 60, 3980−3987 Read Online

ACCESS | Metrics & More | Article Recommendations | Supporting Information

ABSTRACT: Four new tris-Anderson polyoxometalates (POMs), $(NH_4)_4[ZnMo_6O_{18}(C_4H_8NO_3)(OH)_3]\cdot 4H_2O$ (**1**), $(NH_4)_4[CuMo_6O_{18}(C_4H_8NO_3)(OH)_3]\cdot 4H_2O$ (**2**), $(TBA)_3(NH_4)[ZnMo_6O_{17}(C_5H_9O_3)_2(OH)]\cdot 10H_2O$ (**3**) (TBA = *n*-$C_{16}H_{36}N$), and $(NH_4)_4[CuMo_6O_{18}(C_5H_9O_3)_2]\cdot 16H_2O$ (**4**), were synthesized by a microwave-assisted method. Single-crystal X-ray diffraction revealed that **1** and **2** contained a tris (trihydroxyl organic compounds) ligand grafted on one side, while two tris ligands were grafted on two sides to form χ/δ and δ/δ isomers in **3** and **4**, respectively. ^1H and ^{13}C NMR spectra of the χ/δ isomer **3** were obtained for the first time, with six methylenes showing six peaks in the ^1H NMR spectrum and only four peaks in the ^{13}C NMR spectrum. Mass spectrometry monitoring revealed that during the microwave-assistant process the tris ligand can graft onto POMs to form **1**, while tris directly coordinates with metallic heteroatoms to form isopolymolybdates during the conventional reflux synthesis process. In addition, **1**−**4** can catalyze CO_2 with epoxides into cyclic carbonates with high selectivity and yields at an atmospheric pressure of CO_2, which is lower than the pressure of CO_2 in other catalysis using POMs as catalysts. Furthermore, **1**−**4** showed good catalytic stability and cycling properties. Mechanism studies substantiated POMs cocatalyzed with Br^- to improve the catalytic yields.

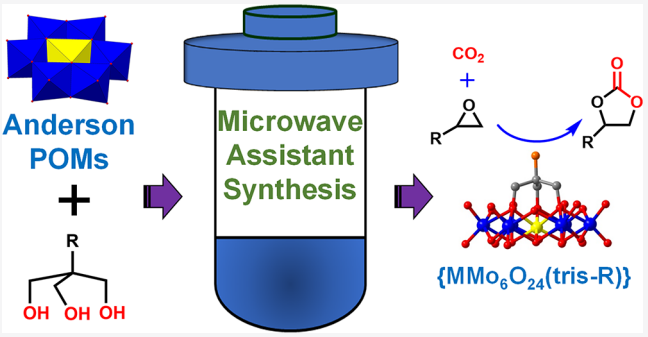

INTRODUCTION

Polyoxometalate (POM) as a traditional inorganic material has been widely studied[1] and used in the fields of optic materials,[2] adsorption materials,[3] electrochemistry,[4] catalysis,[5] biological activity,[6] and so on. In recent years, in order to broaden the application fields of POMs, the combination of POMs with functional organic groups to form new POM-based organic−inorganic hybrid materials becomes the main direction of POM synthesis.[7] One of the common methods of synthesizing the hybrid is to link organic functional groups to POM anions by covalent bonds.[8] This method is beneficial to the design and synthesis of accurate molecular structures[9] and makes POM derivatives diverse.[10] Anderson-type POMs are a kind of classic structure and can be grafted tris (trihydroxyl organic compounds) to obtain functional derivatives,[11] which allow them to have good application prospects in many aspects. For example, Wei's group has done a lot of research on Anderson structural oxidation-catalyzed organic small molecules,[12] and Rompel's group has made a great contribution to the biological applications of Anderson-type POMs.[13] Nevertheless, the application of Anderson POMs is still lacking in some aspects, such as photocatalysis, CO_2 fixation, etc. This is mainly because the synthesis of an Anderson POM-based organic derivative is limited.

So far, there are three ways to add tris to Anderson-type POMs in previous literature: (1) a "one-pot" method using tris, metal salt, and $\{\beta\text{-}Mo_8O_{26}\}$ as starting materials;[14] (2) predesigned Anderson POMs and tris heated to reflux in aqueous solution;[15] (3) using a predesigned Anderson POM step-by-step strategy under hydrothermal conditions.[16] Although lots of work about their synthesis have been done, especially by Wu's group,[17] some structures are still not available by these three ways. For example, unilateral tris substitutions with a central heteroatom, Zn^{2+} or Cu^{2+}, have not been reported, which limits the development of Anderson POM derivatives. Therefore, the search for new synthetic methods to enrich the development of POM organic derivatization is of great significance for POM chemistry.

Microwave-assisted synthesis is different from conventional heating synthesis, which was first carried out in the middle 1980s[18] and widely used in the synthesis the inorganic nanostructure materials in recent years.[19] Compared with traditional synthetic methods, microwave-assisted synthesis has the advantages of short synthesis time, low energy con-

Received: January 5, 2021
Published: February 24, 2021

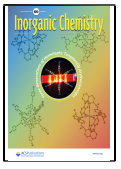

https://dx.doi.org/10.1021/acs.inorgchem.1c00019
Inorg. Chem. 2021, 60, 3980−3987

sumption, and environmental protection.[20] However, microwave-assisted synthesis has received little attention in the synthesis of POMs.[21] In 2016, our group obtained a heteropoly blue, $[(HPO_3)_6Mo_{21}O_{60}(H_2O)_4]^{8-}$, by using a microwave-driven method.[22] However, when traditional heating was used, reduced Keggin-type POM $[PMo_{12}O_{40}]^{4-}$ was obtained instead. In 2018, a new POM-based 2D framework was synthesized by using a microwave and applied for lithium-ion batteries.[23] On the basis of the foundation, we continue to attempt to synthesize new Anderson POM hybrids by microwave-assisted synthesis. Here, we synthesized a series of Anderson POM hybrids by using microwave-assisted synthesis: $(NH_4)_4[ZnMo_6O_{18}(C_4H_8NO_3)(OH)_3]\cdot 4H_2O$ (**1**), $(NH_4)_4[CuMo_6O_{18}(C_4H_8NO_3)(OH)_3]\cdot 4H_2O$ (**2**), $(TBA)_3[ZnMo_6O_{17}(C_5H_9O_3)_2(OH)]\cdot 10H_2O$ (**3**; TBA = *n*-$C_{16}H_{36}N$), and $(NH_4)_4[CuMo_6O_{18}(C_5H_9O_3)_2]\cdot 16H_2O$ (**4**). After comprehensive characterization of these four compounds, it was found that **3** was a χ/δ isomer and showed different NMR spectrs, which was the reported for the first time. The difference of the reaction mechanism between microwave-assisted and conventional heating syntheses was detected by mass spectrometry (MS). Additionally, CO_2 cycloaddition catalysis has been studied, which broadened the application field of Anderson-type POM hybrids.

RESULTS AND DISCUSSION

Synthesis and Structures. In order to obtain the functionalized Anderson-type POMs-based organic−inorganic materials, trihydroxy compounds tris (tris-R, R=NH_2, tris-(hydroxymethyl)methyl aminomethane; R=CH_3, 1,1,1-tris-(hydroxymethyl)ethane) was chosen as the organic model,[24] and series of new functionalized tris-Anderson POMs were synthesized by microwave-assisted predesigned protocol. First, we tried to synthesize unilateral $\{MMo_6(tris\text{-}NH_2)\}$ ($M=Zn^{2+}$ or Cu^{2+}) using traditional heating method as the synthesis method of $\{NiMo_6(tris\text{-}NH_2)\}$,[25] but the products are indeed a large amount of $\{Mo_7O_{24}\}$ (Scheme 1). According to study reported by Rompel and co-workers,[25] unilateral tris-Anderson $\{MMo_6(tris\text{-}NH_2)\}$ cannot be synthesized by "one-pot" protocol because of the coordination of tris-R and metal, which prevents the self-assembly process of Anderson-type POMs and the coordination of tris-NH_2 with POMs. Interestingly, when using the microwave-assisted synthesis method, the desired unilateral substitution structures were obtained as $(NH_4)_4[ZnMo_6O_{18}(C_4H_8NO_3)(OH)_3]\cdot 4(H_2O)$ (**1**) and $(NH_4)_4[CuMo_6O_{18}(C_4H_8NO_3)(OH)_3]\cdot 4(H_2O)$ (**2**). In addition, two new bilateral substituted structures were also synthesized as a χ/δ isomer $(TBA)_3[ZnMo_6O_{17}(C_5H_9O_3)_2(OH)]\cdot 10(H_2O)$ (**3**) and a δ/δ isomer $(NH_4)_4[CuMo_6O_{18}(C_5H_9O_3)_2]\cdot 16(H_2O)$ (**4**) (TBA = *n*-$C_{16}H_{36}N$). It is worth mentioning that **3** and **4** can be generated by conventional reflux method as well, while **1** and **2** cannot be obtained by reflux method. The result indicates that microwave assisted synthesis protocol can be used to synthesis some compounds which cannot be obtained by conventional reflux method.

Single-crystal X-ray diffraction (SCXRD) revealed that **1** crystallizes in the triclinic system with space group $P\bar{1}$. The anions are arranged in a dimer and shown in Figure 1A,E. Six edge-sharing $\{MoO_6\}$ octahedra are around one central $\{ZnO_6\}$ unit. tris-NH_2 caps on one side by occupying three μ_2-O atoms of the $\{ZnO_6\}$ unit. On the other side, μ_2-OH formed hydrogen bonds with μ_3-O of another $[ZnMo_6O_{18}(C_4H_8NO_3)(OH)_3]^{4-}$ anion to form a dimer. Different from the dimers of $\{NiMo_6(tris\text{-}NH_2)\}_2$ and $\{CrMo_6(tris\text{-}CH_2OH)\}_2$ reported previously,[25,26] only four hydrogen bonds are formed between the dimer instead of six. In addition, although the structure of a single anion of **2** is similar to that of **1** (Figure 1B), except for the central structure was changed to a $\{CuMo_6\}$ octahedron. Compound **2** does not form a dimer structure but is connected by hydrogen bonds to form a zigzag-shaped chain structure, as shown in Figure 1F, which is discovered in the tris-Anderson derivative structures for the first time. Two hydrogen bonds are formed between two adjacent anions, and a 1D chain structure is formed. This different arrangement also results in **2** crystallizing in the monoclinic system with space group $P2_1/c$, which is different from **1**. For compounds **3** and **4**, there is no hydrogen bond between the anions because of the different anion structures. One tris-CH_3 molecule in **3** replaces three μ_2-O atoms, and another tris-CH_3 molecule replaces two μ_2-O atoms and one μ_3-O atom to form the χ/δ isomer **3** (Figure 1C). Otherwise, two tris-CH_3 molecules replace six μ_2-O atoms and cap on each side of $\{CuMo_6\}$ to form the δ/δ isomer **4** (Figure 1D). Although much has been reported about the different configurations of tris-Anderson derivatives with the 3+ valence of intermediate heteroatomic metals (Cr^{3+}, Mn^{3+}, Fe^{3+}, etc.), the Anderson structure with the 2+ valence of the intermediate

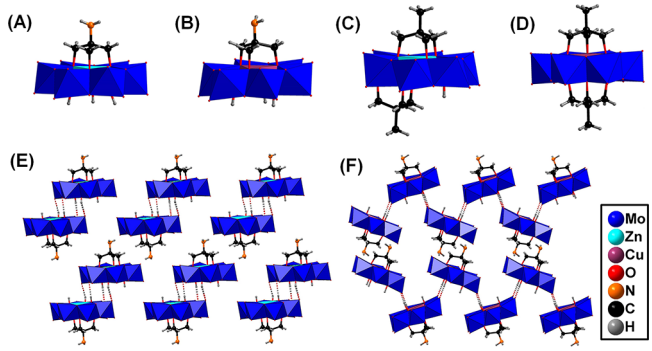

Figure 1. Anion structures of compounds **1** (A), **2** (B), **3** (C), and **4** (D) and the crystal packings of **1** (E) and **2** (F). Cations, solvent molecules, and partial H atoms are removed for clarity.

Scheme 1. Illustration of the Different Synthetic Conditions Affecting the Products[a]

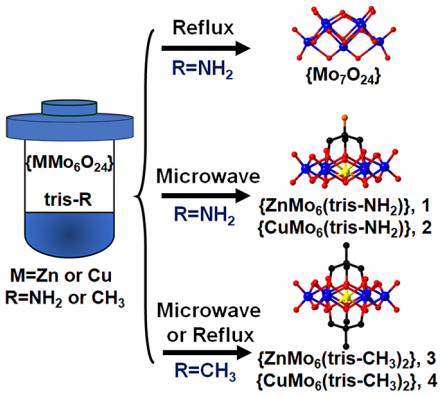

[a]Color code: black, C; red, O; orange, N; blue, Mo; yellow, metal. tris-R = trihydroxyl organic compound.

https://dx.doi.org/10.1021/acs.inorgchem.1c00019
Inorg. Chem. 2021, 60, 3980−3987

heteroatomic metal has not been reported much. For comparison, Figure S3 and Table S2 show several classic structures reported in the previous literature and this paper.

Characteristic. NMR spectra are used to demonstrate the existing states of **1** and **3** in solution. Because of the molecular symmetry of **1**, only two peaks at 4.76 and 4.61 ppm are found (Figure S4), which can be assigned to one amino group and three methylene groups, respectively. Different from **1**, **3** shows six peaks assigned to six methylene groups in the range of 4.07−4.63 ppm (Figure 2A), indicating that the six methylene

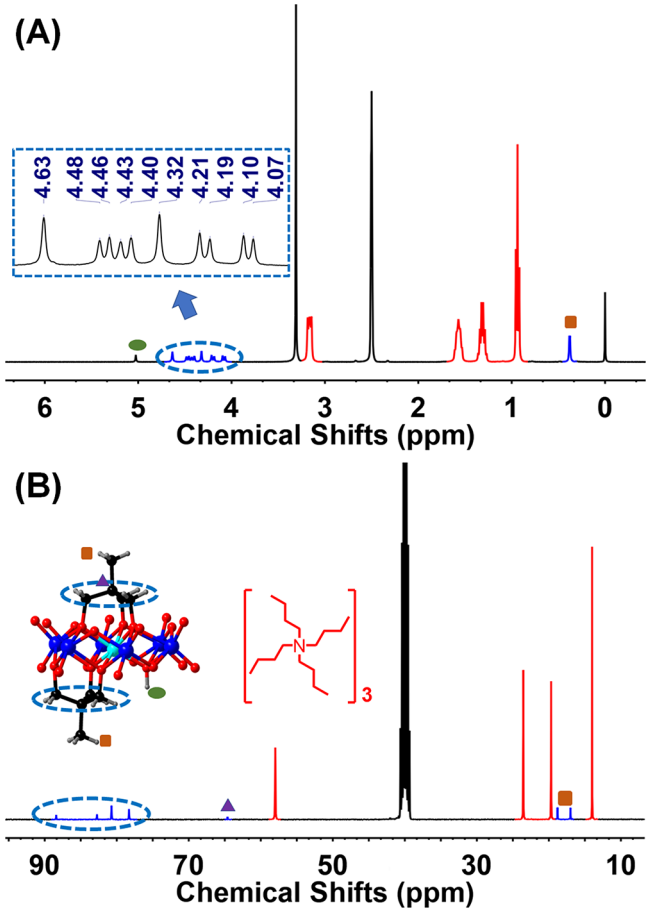

Figure 2. ^{1}H (A) and ^{13}C (B) NMR spectra of **3** in DMSO-d_6.

groups of the χ/δ isomer are in different chemical environments. This is a big difference from the χ/χ isomer, which only shows three methylene peaks.[11a] Besides, a singlet of μ_3-OH can be found at 5.03 ppm (provided in Figure S6), and the peaks of TBA^+ are also shown in the spectrum. The integral ratio of TBA^+ and methylene is 1:12, which verifies that the ratio of anion $[ZnMo_6O_{17}(C_5H_9O_3)_2(OH)]^{3-}$ and cation TBA^+ is 1:3, is consistent with the SCXRD results. Moreover, compared with the ^{1}H NMR spectra of ligands tris-NH_2 and tris-CH_3 (Figures S5 and S7), the chemical peaks of the methylene groups in **1** and **2** shift toward low fields because of the shield effects of metals. In order to figure out where the six methylene peaks in **3** belong, 2D NOESY is carried out (Figure S8). The results show that two double peaks and one single peak can be assigned to one tris-CH_3 ligand. Different from the ^{1}H NMR spectrum, six methylene groups show only four peaks in the ^{13}C NMR spectrum in the range of 75−90 ppm (Figure 2B). In addition, two methyl groups show two singlets, which overlapped most parts (Figure S8), and two chemical shifts in the ^{13}C NMR spectrum (16.99 and 18.80 ppm). The 2D SHQC NMR spectrum (Figure S10) also demonstrates the attribution of different C atoms. To the best of our knowledge, this is the first time to obtain the NMR spectrum of the χ/δ isomer.

Powder X-ray diffraction (PXRD; Figures S12−S15) analysis is used to characterize the purity of the solid samples. Compared with the PXRD spectra simulated from SCXRD, the peaks are matched undifferentiated, which can verify the purity of the compounds. Fourier transform infrared (FT-IR; Figure S16) spectra of compounds **1**−**4** are typical of Anderson-type POMs, and the characteristic peaks observed are consistent with those of previous reports.[27] All compounds displayed similar characteristic Mo−O−Mo and Mo═O vibrations because of the presence of the Anderson-type anion. Taking **1** as an example, the vibrational bands of the terminal Mo═O groups are at about 891 and 808 cm^{-1}, and the vibrational bands of bridging Mo−O−Mo groups are at about 658 cm^{-1}. These peaks are consistent with the typical parent Anderson-type structures. In addition, the peaks of 1118 and 1402 cm^{-1} can be assigned to the C−O and C−H bonds, which belong to the tris-NH_2 part. The thermogravimetric analysis (TGA) and differential scanning calorimetry (DSC) curves show the thermal stability of **1**−**4**, and the molecular formula can be confirmed by the weight loss. In the first stage of the weight loss, it can correspond to the loss of water. Therefore, according to Figure S17, the water of crystallization is figured out, and the molecular formulas of compounds **1**−**4** are confirmed as $(NH_4)_4[ZnMo_6O_{18}(C_4H_8NO_3)(OH)_3]\cdot 4H_2O$, $(NH_4)_4[CuMo_6O_{18}(C_4H_8NO_3)(OH)_3]\cdot 4H_2O$, $(C_{16}H_{36}N)_3[ZnMo_6O_{17}(C_5H_9O_3)_2(OH)]\cdot 10H_2O$, and $(NH_4)_4[CuMo_6O_{18}(C_5H_9O_3)_2]\cdot 16H_2O$, respectively.

Self-Assembly Study. The electrospray ionization mass spectrometry (ESI-MS) spectra were used to obtain information about the structures. The anion peaks can be observed to prove the structures (Figures S18−S21) of the compounds and infer the process of self-assembly.[28] As shown in Figure S22 and Table S3, a series ESI-MS spectra were obtained at different microwave-assisted reaction times. With an increase of the reaction time, a series of small ion fragment peaks disappeared gradually, indicating that the small POM fragments gradually self-assembled into larger ones. Thus, a possible self-assembly process was proposed based on variation of the ion peaks over time and shown in Figure 3. First, $\{ZnMo_6O_{24}\}$ decomposed into small structures ($\{Mo_4O_{13}\}$, $\{Mo_3O_{16}\}$, $\{ZnMo_3O_{11}\}$, and $\{ZnMo_2O_{11}\}$) and finally formed the smallest $\{Mo_2O_7\}$ unit. Second, $\{Mo_2O_7\}$ and tris reassembled to form the $\{(tris)Mo_3O_6\}$, $\{(tris)Mo_4O_9\}$, and $\{(tris)Mo_4O_{11}\}$ structures and then Zn^{2+} was added to obtain $\{(tris)ZnMo_4O_{12}\}$. Finally, compound **1** was formed as the final main product. On the other hand, different MS spectra were also obtained under different conventional heating reaction times and are shown in Figure S23. Different from the microwave reactions, a series of isopolymolybdates were found, while the ions containing Zn^{2+} were not observed. Besides, $[Zn(tris)(H_2O)]^+$ was found at the positive mode, which verified that Zn^{2+} and tris would combine and thus prevent the combination of tris and POMs. With an increase of the reaction time, the gradual disappearance of the small ion fragment peaks indicated that the ions self-assembled into large-structure isopolymolybdates and finally into the stable $\{Mo_7O_{24}\}$. Therefore, two different synthetic methods affect

https://dx.doi.org/10.1021/acs.inorgchem.1c00019
Inorg. Chem. 2021, 60, 3980−3987

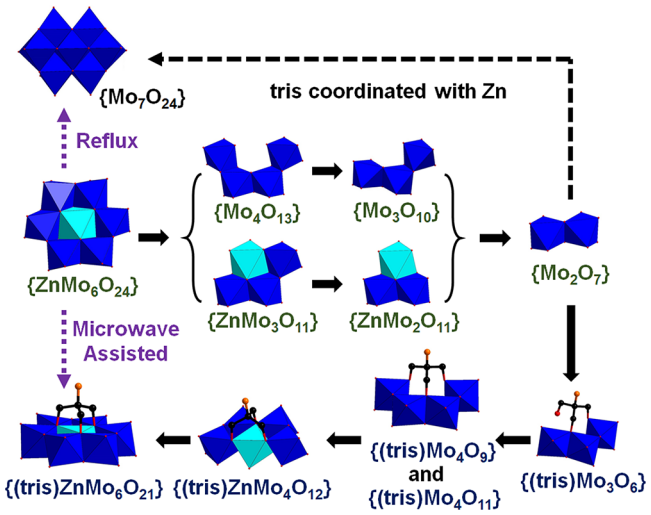

Figure 3. Putative self-assembly mechanism of microwave-assisted and reflux syntheses based on the ESI-MS spectra.

the connection of tris and metals, resulting in different products.

CO_2 Cycloaddition. CO_2 transformation has been a hotspot for a long time.[29] As one of the products, cyclic carbonates have received extensive attention because they can be used as intermediates in fine chemicals, batteries, plastics, etc.[30] However, POMs as conventional catalysts are not widely used in such catalytic reactions, and the catalytic conditions are still harsh.[31] In this work, compounds **1**−**4** were used as catalysts to catalyze the cycloaddition of CO_2 into a cyclic carbonate, and an attempt was made to simplify the catalytic conditions to expand application.

In order to explore the optimal reaction conditions, epichlorohydrin, **1**, and tetrabutylammonium bromide (TBABr) were chosen as the substrate, catalyst, and cocatalyst, respectively. As shown in Table 1, the cocatalyst itself could convert the epoxide and CO_2 into cyclic carbonate in low yield (entry 2). However, the catalyst itself could not convert the epoxide without the cocatalyst (entry 3). In addition, a certain

Table 1. Epichlorohydrin Cycloaddition with CO_2 over Different Conditions[a]

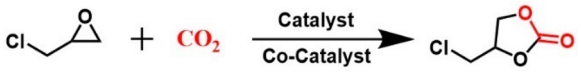

entry	catalyst	cocatalyst (mmol)	pressure (atm)	t (h)	T (°C)	yield (%)[b]
1	**1**	1	1	3	70	99.9
2	none	1	1	3	70	10.3
3	**1**	none	1	3	70	
4	**1**	1	air	3	70	
5	**1**	1	1	3	30	19.8
6	**1**	1	1	3	60	90.3
7	**1**	1	1	2	70	94.7
8	**1**	1	1	1	70	81.7
9	**2**	1	1	3	70	91.3
10	**3**	1	1	3	70	99.9
11	**4**	1	1	3	70	95.2

[a]Reaction conditions: epichlorohydrin, 20 mmol; catalyst, 0.03 mmol (0.15 mol %); cocatalyst, TBABr. [b]Determined by ^{1}H NMR spectroscopy; selectivities were over 99% in all cases.

CO_2 pressure and high temperature have also been verified to be essential in the reaction. It is worth mentioning that the pressure of CO_2 used in the catalytic process is 1 atm, which is much lower than that of the reported catalytic process by other POMs.[31] When the catalytic effects of **1**−**4** were compared, it was found that the catalytic effects of **1** and **3** were better than those of **2** and **4**, indicating that the different heteroatoms in Anderson-type POMs have different effects on the catalytic reaction. In order to explore the stability of **1**−**4**, PXRD and FT-IR analyses were carried out on the catalyst before and after reaction. As shown in Figures S23 and S24, the catalyst did not change before and after catalytic reaction, indicating the stability of **1**−**4**. Moreover, when the catalysts were repeated five times in the reaction, the catalytic yield did not decrease significantly, suggesting that the Anderson-type POMs had a good catalytic performance in the CO_2 cycloaddition reaction. To further explore the cycloaddition catalysis of CO_2 at 1 atm, a series of different substrates were explored, and the results are shown in Table S4. As can be seen, the catalytic performance has a great relationship with the structures of the catalysts. For the same catalyst, different types of catalytic substrates also show different catalytic properties.

As shown in Table 1, entry 2, the reaction can also be carried out with TBABr as the cocatalyst in the solution without catalysts, suggesting that TBABr played an important role in the reaction. According to the literature,[30a] this reaction pathway is the epoxides catalyzed by TBABr. On this basis, the possible mechanism in Figure 4 was proposed. The mechanism

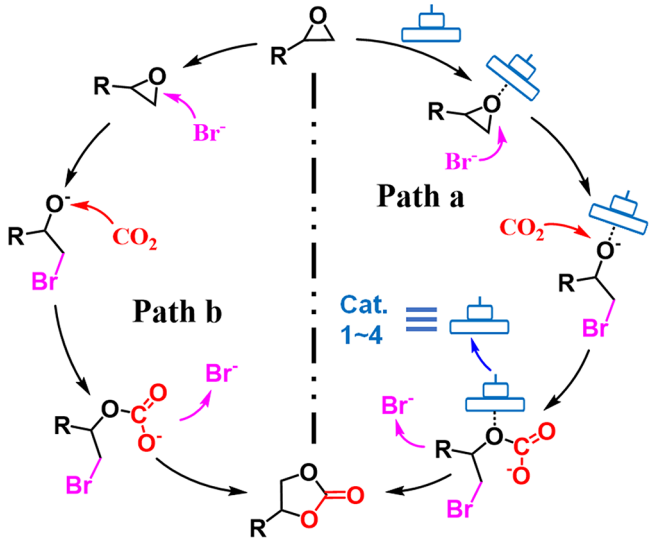

Figure 4. Proposed reaction mechanism for the cycloaddition of CO_2.

can be divided into two pathways, in which Path a is the catalyst by Anderson-type POMs and Path b is the reaction directly catalyzed by TBABr. In Path a, POM was first interacted with epoxide to activate C−O bonds in the substrates (the interaction between POMs and epoxide is shown in Figure S28). The Br^- belonging to TBABr attacks the C−O bond, thus achieving the open-loop reaction of the substrate. Then the C atom at the center of CO_2 attacks the O atom after the open ring and inserts into it. Finally, Br^- leaves after the C−Br bond breaks, and the C and O atoms connect to form the final product, while the POM leaves the substrate and participates in the next catalytic reaction. In Path b, TBABr directly attacks the epoxide substrate without POM

https://dx.doi.org/10.1021/acs.inorgchem.1c00019
Inorg. Chem. 2021, 60, 3980−3987

activation, and the subsequent reaction is similar to that in Path a.

CONCLUSION

Herein, we synthesized a series of tris-grafted Anderson POMs, **1**−**4**, by using a microwave-assisted strategy. Although **3** and **4** can also be synthesized by conventional "one-pot" methods, only **1** and **2** can be obtained by microwave protocol. MS monitoring showed the self-assembly process of the microwave synthesis, while a metal heteroatom would combine with tris during the traditional synthesis, resulting in molybdenum self-assembling into the $\{Mo_7O_{24}\}$ structure. **3** as a χ/δ isomer showed an NMR spectrum different from those of other isomers, in which the six methylene groups showed six peaks in the ^{1}H NMR spectrum and only four peaks in the ^{13}C NMR spectrum. In addition, **1**−**4** can catalyze CO_2 and epoxides into cyclic carbonates with high selectivity and yield under an atmospheric pressure of CO_2, and two possible mechanism pathways were proposed. This work not only explored new microwave-assisted synthesis methods but also provided a catalytic reaction of CO_2 fixation under facile conditions.

EXPERIMENTAL SECTION

Materials and Physical Measurement. All reagents were purchased from commercial sources and used without further purification except those specifically noted. The NMR spectra were performed on a Bruker Avance 400 MHz spectrometer in Deuterium generation reagent with tetramethylsilane as the inner standard. FT-IR spectra were obtained on an Alpha Centauri FT-IR spectrometer in the 400−4000 cm^{-1} region with a KBr pellet. TGA−DSC was performed on a PerkinElmer TGA7 instrument under flowing Ar, and the temperature was set from 40 to 800 °C under a heating rate of 10 °C/min with an Ar flow of 25 mL/min. ESI-MS spectra were recorded with a Bruker Compact quadrupole time-of-flight (QTOF) mass spectrometer with an electrospray ionizer, and data analysis was performed on a Bruker IsotopePattern. PXRD was employed using Cu Kα in the range of 10−50° with a scanning rate of 10°/min. The crystallographic data and structural refinements are given in Table S1. SCXRD analysis was performed on a Bruker APEX-II diffractometer with graphite-monochromated Mo Kα radiation at 296 K (λ = 0.71073 Å). A multiscan technique was used for absorption correction. Using *Olex2*, the structure was solved with the *ShelXT* structure solution program using intrinsic phasing and refined with the *ShelXL* refinement package using least-squares minimization.[32] CCDC 2053657, 2053743, 2053744, and 2053745 contain the supplementary crystallographic data for this paper. $(NH_4)_4[ZnMo_6O_{24}H_6]\cdot 5H_2O$ ({**ZnMo$_6$**}) and $(NH_4)_4[CuMo_6O_{24}H_6]\cdot 5H_2O$ ({**CuMo$_6$**}) were synthesized according to a previous report.[33] The solubility tests in different solvents and stability tests in water with pH values of **1**−**4** are shown in the Supporting Information.

Microwave-Assisted Synthesis of $(NH_4)_4[ZnMo_6O_{18}(C_4H_8NO_3)(OH)_3]\cdot 4H_2O$ (1). $(NH_4)_4[ZnMo_6O_{24}H_6]\cdot 5H_2O$ (1.1 g, 0.92 mmol) and $(CH_2OH)_3CNH_2$ (0.12 g, 1 mmol) were placed in a sealed glass tube containing 15 mL of deionized water and dissolved ultrasonically, and the resulting solution was then placed in a microwave reactor. The reaction mixture was heated to 140 °C for 10 min and maintained at 140 °C with a microwave power of 30 W for 30 min. After cooling to room temperature, the mixture was filtered and a white block-shaped crystal was obtained in a few days (52% yield, based on Mo). ^{1}H NMR (DMSO-d_6, 400 MHz): δ 6.81 (s, 6H), 3.17 (t, 3H), 1.57 (m, 2H), 1.32 (m, 2H), 0.94 (t, 3H). IR (KBr, cm^{-1}): 1631 (s), 1402 (vs), 891 (vs), 808 (w), 657 (s), 571 (w), 479 (w). ESI-MS $[\{(TBA)_2[ZnMo_6O_{24}H_3((CH_2)_3CNH_2)](H_2O)\}^{2-}]$. Found: m/z 800.47. Theoretical: m/z 800.46. ICP-OES: Mo, 0.466 (calcd, 0.464); Zn, 0.055 (calcd, 0.053). Elem anal. Found (calcd): C, 0.041 (0.039); H, 0.031 (0.028); N, 0.055 (0.056).

Microwave-Assisted Synthesis of $(NH_4)_4[CuMo_6O_{18}(C_4H_8NO_3)(OH)_3]\cdot 4H_2O$ (2). $(NH_4)_4[CuMo_6O_{24}H_6]$ (1.2 g, 1 mmol) and $(CH_2OH)_3CNH_2$ (0.12 g, 1 mmol) were placed in a sealed glass tube containing 20 mL of deionized water and dissolved ultrasonically, and the resulting solution was then placed in a microwave reactor. The reaction mixture was heated to 140 °C for 10 min and maintained at 140 °C with a microwave power of 30 W for 30 min. After cooling to room temperature, the mixture was filtered and a blue block-shaped crystal was obtained in a few days (45% yield, based on Mo). IR (KBr, cm^{-1}): 1635 (s), 1402 (vs), 889 (s), 804 (w), 648 (s), 577 (w), 474 (w). ESI-MS $[(TBA)_2[CuMo_6O_{24}H_3((CH_2)_3CNH_2)](H_2O)^{2-}]$. Found: m/z 799.92. Theoretical: m/z 799.96. ICP-OES: Mo, 0.461 (calcd, 0.464); Cu, 0.049 (calcd, 0.051). Elem anal. Found (calcd): C, 0.034 (0.039); H, 0.030 (0.028); N, 0.054 (0.056).

Microwave-Assisted Synthesis of $(C_{16}H_{36}N)_3[ZnMo_6O_{17}(C_5H_9O_3)_2(OH)]\cdot 10H_2O$ (3). $(NH_4)_4[ZnMo_6O_{24}H_6]\cdot 5H_2O$ (1.1 g, 0.92 mmol) and $(CH_2OH)_3CCH_3$ (0.24 g, 2 mmol) were placed in a sealed glass tube containing 25 mL of deionized water and dissolved ultrasonically, and the resulting solution was then placed in a microwave reactor. The reaction mixture was heated to 140 °C for 10 min and maintained at 140 °C with a microwave power of 30 W for 30 min. After cooling to room temperature, TBABr (0.5 g, 1.5 mmol) was added. The mixture was filtered, and a white block-shaped crystal was obtained in a few days (65% yield, based on Mo). ^{1}H NMR (DMSO-d_6, 400 MHz): δ 4.63 (s, 2H), 4.48−4.40 (m, 4H), 4.32 (s, 2H), 4.20 (d, 2H), 4.08 (d, 2H), 3.17 (t, 3H), 1.57 (m, 2H), 1.32 (m, 2H), 0.94 (t, 3H). IR (KBr, cm^{-1}): 2964 (s), 2867 (s), 1653 (s), 1471 (s), 1396 (w), 1114 (w), 1030 (s), 923 (s), 665 (s), 595 (s), 543 (w). ESI-MS $[(TBA)_2H[ZnMo_6O_{24}(C_3H_6CCH_3)_2H]^-]$. Found: m/z 1649.98. Theoretical: m/z 1649.96. ESI-MS $[(TBA)_3[ZnMo_6O_{24}(C_3H_6CCH_3)_2H]^-]$. Found: m/z 1891.26. Theoretical: m/z 1891.25. ICP-OES: Mo, 0.281 (calcd, 0.275); Zn, 0.029 (calcd, 0.031). Elem anal. Found (calcd): C, 0.302 (0.333); H, 0.078 (0.072); N, 0.026 (0.027).

Microwave-Assisted Synthesis of $(NH_4)_4[CuMo_6O_{18}(C_5H_9O_3)_2]\cdot 16H_2O$ (4). $(NH_4)_4[CuMo_6O_{24}H_6]$ (0.35 g, 0.29 mmol) and $(CH_2OH)_3CCH_3$ (0.06 g, 0.5 mmol) were placed in a sealed glass tube containing 10 mL of deionized water and dissolved ultrasonically, and the resulting solution was then placed in a microwave reactor. The reaction mixture was heated to 140 °C for 10 min and maintained at 140 °C with a microwave power of 30 W for 30 min. After the solvent cooled to room temperature, TBABr (0.24 g, 0.75 mmol) was added. The mixture was filtered, and a blue block-shaped crystal was obtained in a few days (63% yield, based on Mo). IR (KBr, cm^{-1}): 2967 (w), 2859 (w), 1647 (s), 1465 (s), 1403 (s), 1113 (w), 1033 (s), 925 (s), 650 (s), 563 (w). ESI-MS $[(TBA)H_2[CuMo_6O_{24}(C_{16}H_{36}CCH_3)_2]^-]$. Found: m/z 1406.48. Theoretical: m/z 1406.48. ESI-MS $[(TBA)_2H[CuMo_6O_{24}(C_{16}H_{36}CCH_3)_2]^-]$. Found: m/z 1647.96. Theoretical: m/z 1647.96. ESI-MS $[(TBA)_3[CuMo_6O_{24}(C_{16}H_{36}CCH_3)_2]^-]$. Found: m/z 1889.24. Theoretical: m/z 1889.24. ICP-OES: Mo, 0.390 (calcd, 0.387); Cu, 0.040 (calcd, 0.042). Elem anal. Found (calcd): C, 0.077 (0.079); H, 0.045 (0.043); N, 0.034 (0.037).

Traditional Heating Method. $(NH_4)_4[MMo_6O_{24}H_6]\cdot 5H_2O$ (M═Zn or Cu, 0.92 mmol) and $(CH_2OH)_3CNH_2$ (1 mmol) were placed in a round flask containing 20 mL of deionized water and dissolved ultrasonically. The reaction mixture was heated to reflux for 12 h. After cooling to room temperature, the mixture was filtered and a white block-shaped crystal was obtained in a few days (70% yield, based on Mo). The crystal was analyzed as $(NH_4)[Mo_7O_{24}]$ by a SCXRD test. In particular, although **3** and **4** can be obtained by conventional heating, the compounds used in this paper were synthesized by a microwave-assisted synthesis.

$(NH_4)_4[ZnMo_6O_{24}H_6]\cdot 5H_2O$ (0.92 mmol) and $(CH_2OH)_3CCH_3$ (2 mmol) were placed in a round flask containing 25 mL of deionized water and dissolved ultrasonically. The reaction mixture was heated to

https://dx.doi.org/10.1021/acs.inorgchem.1c00019
Inorg. Chem. 2021, 60, 3980−3987

reflux for 12 h. After cooling to room temperature, TBABr (1.5 mmol) was added. The mixture was filtered, and a white block-shaped crystal was obtained in a few days (71% yield, based on Mo). The crystal was analyzed as $(TBA)_3(NH_4)[ZnMo_6O_{17}(C_5H_9O_3)_2(OH)]\cdot 10(H_2O)$ (**3**) by a SCXRD test.

$(NH_4)_4[CuMo_6O_{24}H_6]$ (0.29 mmol) and $(CH_2OH)_3CCH_3$ (0.5 mmol) were placed in a round flask containing 25 mL of deionized water and dissolved ultrasonically, and the reaction mixture was heated to reflux for 12 h. After the solvent cooled to room temperature, TBABr (0.75 mmol) was added. The mixture was filtered, and a blue block-shaped crystal was obtained in a few days (60% yield, based on Mo). The crystal was analyzed as $(NH_4)_4[CuMo_6O_{18}(C_5H_9O_3)_2]\cdot 16(H_2O)$ (**4**) by a SCXRD test.

CO_2 Cycloaddition. The corresponding epoxide (20 mmol), catalyst (0.03 mmol, 0.15 mol %), and TBABr (0.32 g, 1 mmol) were added to an Erlenmeyer flask. After the bottle was full of CO_2, which was achieved by using balloons and a three-way valve, the solution was stirred at 70 °C for 3 h. The productivity was calculated by using ^1H NMR. After the reaction, CH_2Cl_2 was added to the solution to precipitate the catalyst. Then the precipitate was filtered, and the impurities were washed away with a large amount of CH_2Cl_2. After drying, the catalyst was recovered and used for the next cycles.

■ ASSOCIATED CONTENT

Supporting Information

The Supporting Information is available free of charge at https://pubs.acs.org/doi/10.1021/acs.inorgchem.1c00019.

Details of SCXRD, NMR spectra, PXRD, FT-IR, TGA and DSC, ESI-MS, and CO_2 cycloaddition, and solubility tests in different solvents and stability tests in H_2O with pH values, including Figures S1−S54 and Tables S1−S7 (PDF)

Accession Codes

CCDC 2053657 and 2053743−2053745 contain the supplementary crystallographic data for this paper. These data can be obtained free of charge via www.ccdc.cam.ac.uk/data_request/cif, or by emailing data_request@ccdc.cam.ac.uk, or by contacting The Cambridge Crystallographic Data Centre, 12 Union Road, Cambridge CB2 1EZ, UK; fax: +44 1223 336033.

■ AUTHOR INFORMATION

Corresponding Authors

Wei-Dong Yu − *Hunan Institute of Nuclear Agricultural Science and Space Breeding, Hunan Academy of Agricultural Science, Changsha 410000, P. R. China;* orcid.org/0000-0001-6937-6944; Email: fenly18@sina.com

Jun Yan − *School of Chemistry and Chemical Engineering, Central South University, Changsha 410000, P. R. China;* orcid.org/0000-0002-6158-0614; Email: yanjun@csu.edu.cn

Authors

Yin Zhang − *Junior Education Department, Changsha Normal University, Changsha 410100, P. R. China*

Yu-Yang Han − *School of Chemistry and Chemical Engineering, Central South University, Changsha 410000, P. R. China*

Bin Li − *School of Chemistry and Chemical Engineering, Central South University, Changsha 410000, P. R. China*

Sai Shao − *Hunan Institute of Nuclear Agricultural Science and Space Breeding, Hunan Academy of Agricultural Science, Changsha 410000, P. R. China*

Le-Ping Zhang − *Hunan Institute of Nuclear Agricultural Science and Space Breeding, Hunan Academy of Agricultural Science, Changsha 410000, P. R. China*

Hong-Ke Xie − *Hunan Institute of Nuclear Agricultural Science and Space Breeding, Hunan Academy of Agricultural Science, Changsha 410000, P. R. China*

Complete contact information is available at: https://pubs.acs.org/10.1021/acs.inorgchem.1c00019

Funding

This work was supported by the Natural Science Foundation of Hunan Province (Grant 2020JJ4684).

Notes

The authors declare no competing financial interest.

■ REFERENCES

(1) (a) Pope, M. T.; Müller, A. Polyoxometalate chemistry: an old field with new dimensions in several disciplines. *Angew. Chem., Int. Ed. Engl.* **1991**, *30*, 34−38. (b) Long, D. L.; Burkholder, E.; Cronin, L. Polyoxometalate clusters, nanostructures and materials: from self assembly to designer materials and devices. *Chem. Soc. Rev.* **2007**, *36*, 105−121.

(2) Chen, L.; Chen, W. L.; Wang, X. L.; Li, Y. G.; Su, Z. M.; Wang, E. B. Polyoxometalates in dye-sensitized solar cells. *Chem. Soc. Rev.* **2019**, *48*, 260−284.

(3) Li, J. H.; Wang, X. L.; Song, G.; Lin, H. Y.; Wang, X.; Liu, G. C. Various Anderson-type polyoxometalate-based metal-organic complexes induced by diverse solvents: assembly, structures and selective adsorption for organic dyes. *Dalton Trans.* **2020**, *49*, 1265−1275.

(4) (a) Jia, X.; Wang, J.; Hu, H.; Song, Y. F. Three-dimensional carbon framework anchored polyoxometalate as a high-performance anode for lithium-ion batteries. *Chem. - Eur. J.* **2020**, *26*, 5257−5263. (b) Du, J.; Lang, Z. L.; Ma, Y. Y.; Tan, H. Q.; Liu, B. L.; Wang, Y. H.; Kang, Z. H.; Li, Y. G. Polyoxometalate-base electron transfer modulation for efficient electrocatalytic carbon dioxide reduction. *Chem. Sci.* **2020**, *11*, 3007−3015.

(5) (a) Samaniyan, M.; Mirzaei, M.; Khajavian, R.; Eshtiagh-Hosseini, H.; Streb, C. Heterogeneous catalysis by polyoxometalates in metal-organic frameworks. *ACS Catal.* **2019**, *9*, 10174−10191. (b) Wang, S. S.; Yang, G. Y. Recent advances in polyoxometalate-catalyzed reactions. *Chem. Rev.* **2015**, *115*, 4893−4962.

(6) (a) Bijelic, A.; Aureliano, M.; Rompel, A. Polyoxometalates as potential next-generation metallodrugs in the combat against cancer. *Angew. Chem., Int. Ed.* **2019**, *58*, 2980−2999. (b) Blazevic, A.; Al-Sayed, E.; Roller, A.; Giester, G.; Rompel, A. Tris-functionalized hybrid Anderson polyoxometalates: synthesis, characterization, hydrolytic stability and inversion of protein surface charge. *Chem. - Eur. J.* **2015**, *21*, 4762−4771.

(7) (a) Dolbecq, A.; Dumas, E.; Mayer, C. R.; Mialane, P. Hybrid organic-inorganic polyoxometalate compounds: from structural diversity to applications. *Chem. Rev.* **2010**, *110*, 6009−6048. (b) Li, C. F.; Mizuno, N.; Yamaguchi, K.; Suzuki, K. Self-assembly of anionic polyoxometalate-organic architectures based on lacunary phosphomolybdates and pyridyl ligands. *J. Am. Chem. Soc.* **2019**, *141*, 7687−7692. (c) Yang, X. X.; Yu, W. D.; Yi, X. Y.; Liu, C. Accurate regulating of visible-light absorption in polyoxotitanate-calix[8]arene systems by ligand modification. *Inorg. Chem.* **2020**, *59*, 7512−7519. (d) Yang, X. X.; Yu, W. D.; Yi, X. Y.; Li, L. J.; Liu, C. Monocarboxylate-driven structural growth in calix[n]arene-polyoxotitanate hybrid systems: utility in hydrogen production from water. *Chem. Commun.* **2020**, *56*, 14035−14038. (e) Yu, W.; Li, B.; Zhang, Y.; Yan, Q.; Yan, J. Discovery of a fullerene-polyoxometalate hybrid exhibiting enhanced photocurrent response. *Inorg. Chem.* **2020**, *59*, 5266−5270.

(8) (a) Xu, Q. H.; Yuan, S. S.; Zhu, L.; Hao, J.; Wei, Y. G. Synthesis of novel bis(Triol)-functionalized Anderson clusters serving as potential synthons for forming organic-inorganic hybrid chains. *Chem. Commun.* **2017**, *53*, 5283−5286. (b) Diab, M.; Mateo, A.; Al

Cheikh, J.; Haouas, M.; Ranjbari, A.; Bourdreux, F.; Naoufal, D.; Cadot, E.; Bo, C.; Floquet, S. Unprecedented coupling reaction between two anionic species of a *closo*-decahydrodecaborate cluster and an Anderson-type polyoxometalate. *Dalton Trans.* **2020**, *49*, 4685−4689.

(9) (a) Luo, Y.; Maloul, S.; Wächtler, M.; Winter, A.; Schubert, U. S.; Streb, C.; Dietzek, B. Is electron ping-pong limiting the catalytic hydrogen evolution activity in covalent photosensitizer-polyoxometalate dyads. *Chem. Commun.* **2020**, *56*, 10485−10488. (b) Li, X. H.; Liu, Y. W.; Lu, Y.; Zhang, Z.; Tian, H. R.; Liu, S. M.; Liu, S. X. A universal strategy for fabrication and morphology control of polyoxometalate-based metal-organic frameworks. *Chem. Commun.* **2020**, *56*, 1641−1644.

(10) (a) Zhang, J. W.; Huang, Y. C.; Li, G.; Wei, Y. G. Recent advances in alkoxylation chemistry of polyoxometalates: from synthetic strategies, structural overviews to functional applications. *Coord. Chem. Rev.* **2019**, *378*, 395−414. (b) Anyushin, A. V.; Kondinski, A.; Parac-Vogt, T. V. Hybrid polyoxometalates as post-functionalization platforms: from fundamentals to emerging applications. *Chem. Soc. Rev.* **2020**, *49*, 382−432. (c) Li, X. X.; Zhao, D.; Zheng, S. T. Recent advances in POM-organic frameworks and POM-organic polyhedral. *Coord. Chem. Rev.* **2019**, *397*, 220−240.

(11) (a) Hasenknopf, B.; Delmont, R.; Herson, P.; Gouzerh, P. Aderson-type heteropolymolybdates containing tris(alkoxo) ligands: synthesis and structural characterization. *Eur. J. Inorg. Chem.* **2002**, *12*, 1081−1087. (b) Marcoux, P. R.; Hasenknopf, B.; Vaissermann, J.; Gouzerh, P. Developing remote metal binding sites in hetero-polymolybdates. *Eur. J. Inorg. Chem.* **2003**, *13*, 2406−2412. (c) Debela, A. M.; Ortiz, M.; Beni, V.; Thorimbert, S.; Lesage, D.; Cole, R. B.; O'Sullivan, C. K.; Hasenknopf, B. Biofunctionalization of polyoxometalates with DNA primers, their use in the polymerase chain reaction (PCR) and electrochemical detection of PCR products. *Chem. - Eur. J.* **2015**, *21*, 17721−17727. (d) Li, X. X.; Ma, X.; Zheng, W. X.; Qi, Y. J.; Zheng, S. T.; Yang, G. Y. Composite hybrid cluster built from the integration of polyoxometalate and a metal halide cluster: synthetic strategy, structure, and properties. *Inorg. Chem.* **2016**, *55*, 8257−8259. (e) Song, Y. F.; Long, D. L.; Cronin, L. Noncovalently connected frameworks with nanoscale channels assembled from a tethered polyoxometalate-pyrene hybrid. *Angew. Chem., Int. Ed.* **2007**, *46*, 3900−3904. (f) Gao, N.; Du, Z.; Guan, Y. J.; Dong, K.; Ren, J. S.; Qu, X. G. Chirality-selected chemical modulation of amyloid aggregation. *J. Am. Chem. Soc.* **2019**, *141*, 6915−6921. (g) Mukhacheva, A. A.; Volchek, V. V.; Yanshole, V. V.; Kompankov, N. B.; Gushchin, A. L.; Benassi, E.; Abramov, P. A.; Sokolov, M. N. Is it possible to prepare a heterometal Anderson-Evans type anion? *Inorg. Chem.* **2020**, *59*, 2116−2120.

(12) (a) Yu, H.; Wang, J. J.; Zhai, Y. Y.; Zhang, M. Q.; Ru, S.; Han, S.; Wei, Y. G. Visible-light-driven photocatalytic oxidation of organic chlorides using air and an inorganic-ligand supported nickel-catalyst without photosensitizers. *ChemCatChem* **2018**, *10*, 4274−4279. (b) Yu, H.; Zhai, Y. Y.; Dai, G. Y.; Ru, S.; Han, S.; Wei, Y. G. Transition-metal-controlled inorganic ligand-supported non-precious metal catalysts for the aerobic oxidation of amines to lmines. *Chem. - Eur. J.* **2017**, *23*, 13883−13887. (c) Zhang, M. Q.; Zhai, Y. Y.; Ru, S.; Zang, D. J.; Han, S.; Yu, H.; Wei, Y. G. Highly practical and efficient preparation of aldehydes and ketones from aerobic oxidation of alcohols with an inorganic-ligand supported iodine catalyst. *Chem. Commun.* **2018**, *54*, 10164−10167. (d) Yu, H.; Ru, S.; Dai, G. Y.; Zhai, Y. Y.; Lin, H. L.; Han, S.; Wei, Y. Y. An efficient iron(III)-catalyzed aerobic oxidation of aldehydes in water for the green preparation of carboxylic acids. *Angew. Chem., Int. Ed.* **2017**, *56*, 3867−3871. (e) Wei, Z. Y.; Ru, S.; Zhao, Q. X.; Yu, H.; Zhang, G.; Wei, Y. G. Highly efficient and practical aerobic oxidation of alcohols by inorganic-ligand supported copper catalysis. *Green Chem.* **2019**, *21*, 4069−4075.

(13) (a) Blazevic, A.; Rompel, A. The Anderson-Evans polyoxometalate: from inorganic building blocks *via* hybrid organic-inorganic structures to tomorrows "Bio-POM". *Coord. Chem. Rev.* **2016**, *307*, 42−64. (b) Schönweiz, S.; Heiland, M.; Anjass, M.; Jacob, T.; Rau, S.; Streb, C. Experimental and theoretical investigation of the light-driven hydrogen evolution by polyoxometalate-photosensitizer dyads. *Chem. - Eur. J.* **2017**, *23*, 15370−15376.

(14) (a) Macdonell, A.; Johnson, N. A. B.; Surman, A. J.; Cronin, L. Configurable nanosized metal oxide oligomers via precise "Click" coupling control of hybrid polyoxometalates. *J. Am. Chem. Soc.* **2015**, *137*, 5662−5665. (b) Musumeci, C.; Rosnes, M. H.; Giannazzo, F.; Symes, M. D.; Cronin, L.; Pignataro, B. Smart high-κ nanodielectrics using solid supported polyoxometalate-rich nanostructures. *ACS Nano* **2011**, *5*, 9992−9999. (c) Yin, P. C.; Zhang, J.; Li, T.; Zuo, X. B.; Hao, J.; Warner, A. M.; Chattopadhyay, S.; Shibata, T.; Wei, Y. G.; Liu, T. B. Self-recognition of structurally identical, rod-shaped macroions with different central metal atoms during their assembly process. *J. Am. Chem. Soc.* **2013**, *135*, 4529−4536. (d) Santoni, M. P.; Pal, A. K.; Hanan, G. S.; Proust, A.; Hasenknopf, B. Discrete covalent organic-inorganic hybrids: terpyridine functionalized polyoxometalates obtained by a modular strategy and their metal complexation. *Inorg. Chem.* **2011**, *50*, 6737−6745.

(15) (a) Ai, H.; Wang, Y.; Li, B.; Wu, L. X. Synthesis and characterization of single-side organically grafted Anderson-type polyoxometalates. *Eur. J. Inorg. Chem.* **2014**, *17*, 2766−2772. (b) Blazevic, A.; Al-Sayed, E.; Roller, A.; Giester, G.; Rompel, A. Tris-functionalized hybrid Anderson polyoxometalates: synthesis, characterization, hydrolytic stability and inversion of protein surface charge. *Chem. - Eur. J.* **2015**, *21*, 4762−4771. (c) Zhang, J. W.; Liu, Z. H.; Huang, Y. C.; Zhang, J.; Hao, J.; Wei, Y. G. Unprecedented χ isomers of single-side triol-functionalized Anderson polyoxometalates and their proton-controlled isomer transformation. *Chem. Commun.* **2015**, *51*, 9097−9100.

(16) (a) Lin, C. G.; Chen, W.; Long, D. L.; Cronin, L.; Song, Y. F. Step-by-step covalent modification of Cr-templated Anderson-type polyoxometalates. *Dalton Trans.* **2014**, *43*, 8587−8590. (b) Zhang, J. W.; Luo, J. H.; Wang, P. M.; Ding, B.; Huang, Y. C.; Zhao, Z. L.; Zhang, J.; Wei, Y. G. Step-by-step strategy from achiral precursors to polyoxometalates-based chiral organic-inorganic hybrids. *Inorg. Chem.* **2015**, *54*, 2551−2559.

(17) (a) Wang, Y.; Li, B.; Qian, H. J.; Wu, L. X. Controlled triol-derivative bonding and decoration transformation on Cu-centered Anderson-Evans polyoxometalates. *Inorg. Chem.* **2016**, *55*, 4271−4277. (b) Wang, Y.; Liu, X. T.; Xu, W.; Yue, Y.; Li, B.; Wu, L. X. Triol-ligand modification and structural transformation of Anderson-Evans oxomolybdates via modulating oxidation state of Co-heteroatom. *Inorg. Chem.* **2017**, *56*, 7019−7028. (c) Wang, Y.; Kong, X. P.; Xu, W.; Jiang, F. R.; Li, B.; Wu, L. X. Ratio-controlled precursors of Anderson-Evans polyoxometalates: synthesis, structural transformation, and magnetic and catalytic properties of a series of triol ligand-decorated $\{M_2Mo_6\}$ clusters ($M{=}Cu^{2+}$, Co^{2+}, Ni^{2+}, Zn^{2+}). *Inorg. Chem.* **2018**, *57*, 3731−3741. (d) Zhang, B.; Yue, L.; Wang, Y.; Yang, Y.; Wu, L. X. A novel single-side azobenzene-grafted Anderson-type polyoxometalate for recognition-induced chiral migration. *Chem. Commun.* **2014**, *50*, 10823−10826.

(18) (a) Komarneni, S.; Roy, R. Titania gel spheres by a new sol-gel process. *Mater. Lett.* **1985**, *3*, 165−167. (b) Gedye, R.; Smith, F.; Westaway, K.; Ali, H.; Baldisera, L.; Laberge, L.; Rousell, J. The use of microwave ovens for rapid organic synthesis. *Tetrahedron Lett.* **1986**, *27*, 279−282.

(19) (a) Zhu, Y. J.; Chen, F. Microwave-assisted preparation of inorganic nanostructures in liquid phase. *Chem. Rev.* **2014**, *114*, 6462−6555. (b) Laybourn, A.; Katrib, J.; Ferrari-John, R. S.; Morris, C. G.; Yang, S.; Udoudo, O.; Easun, T. L.; Dodds, C.; Champness, N. R.; Kingman, S. M.; Schröder, M. Metal-organic frameworks in seconds *via* selective microwave heating. *J. Mater. Chem. A* **2017**, *5*, 7333−7338. (c) Wingen, L. M.; Scholz, M. S. *B*-Cyanodicarba-*closo*-dodecaboranes: facile synthesis and spectroscopic features. *Inorg. Chem.* **2016**, *55*, 8274−8276.

(20) (a) Patete, J. M.; Peng, X. H.; Koenigsmann, C.; Xu, Y.; Karn, B.; Wong, S. S. Visible methodologies for the synthesis of high-quality nanostructures. *Green Chem.* **2011**, *13*, 482−519. (b) Dahl, J. A.;

https://dx.doi.org/10.1021/acs.inorgchem.1c00019
Inorg. Chem. 2021, 60, 3980−3987

Maddux, B. L. S.; Hutchison, J. E. Toward greener nanosynthesis. *Chem. Rev.* **2007**, *107*, 2228−2269.
(21) (a) Bagno, A.; Bonchio, M.; Sartorel, A.; Scorrano, G. Microwave-assisted rapid incorporation of ruthenium into lacunary Keggin-type polyoxotungstates: one-step synthesis, ^{99}Ru, ^{183}W NMR characterization and catalytic activity of $[PW_{11}O_{39}Ru^{II}(DMSO)]^{5-}$. *Eur. J. Inorg. Chem.* **2000**, *2000*, 17−20. (b) Besson, C.; Chen, S. W.; Villanneau, R.; Izzet, G.; Proust, A. A new synthetic route towards Ru(III) substituted heteropolytungstate anion. *Inorg. Chem. Commun.* **2009**, *12*, 1042−1044. (c) Farhadi, S.; Mahmoudi, F.; Simpson, J. A new nano-scale manganese(II) coordination polymer constructed from semicarbzaone Schiff base and dicyanamide ligands: synthesis, crystal structure and DFT calculations. *J. Mol. Struct.* **2016**, *1108*, 583−589. (d) Farhadi, S.; Mahmoudi, F.; Dusek, M.; Eigner, V.; Kucerakova, M. A new inorganic-organic nanohybrid based on a copper(II) semicarbazone complex and the $PMo_{12}O_{40}^{3-}$ polyanion: synthesis, characterization, crystal structure and photocatalytic activity for degradation of cationic dyes. *Polyhedron* **2017**, *122*, 247−256. (e) Ritchie, C.; Bryant, G. Microwave assisted synthesis of a mono organoimido functionalized Anderson polyoxometalate. *Dalton Trans.* **2015**, *44*, 20826−20829.
(22) Jin, X. X.; Yu, W. D.; Nie, Y. M.; Liu, M. S.; Yan, J. $[(HPO_3)_6Mo_{21}O_{60}(H_2O)_4]^{8-}$: a new redox active heteropoly blue cluster with layered shape containing a phosphite template that self-assembles under controlled microwave irradiation. *Dalton Trans.* **2016**, *45*, 3268−3271.
(23) Nie, Y. M.; Liang, S.; Yu, W. D.; Yuan, H.; Yan, J. Microwave-assisted preparation and characterization of a polyoxometalate-based inorganic 2D framework anode for enhancing lithium-ion battery performance. *Chem. - Asian J.* **2018**, *13*, 1199−1205.
(24) Santoni, M.; Hanan, G. S.; Hasenknopf, B. Covalent multi-component systems of polyoxometalates and metal complexes: towards multi-functional organic- inorganic hybrids in molecular and material sciences. *Coord. Chem. Rev.* **2014**, *281*, 64−85.
(25) Gumerova, N. I.; Roller, A.; Rompel, A. Synthesis and characterization of the first nickel(II)-centered single-side tris functionalized Aderson-type polyoxomolybdate. *Eur. J. Inorg. Chem.* **2016**, *36*, 5507−5511.
(26) Wu, P. F.; Yin, P. C.; Zhang, J.; Hao, J.; Xiao, Z. C.; Wei, Y. G. Single-side organically functionalized Anderson-type polyoxometalates. *Chem. - Eur. J.* **2011**, *17*, 12002−12005.
(27) (a) Zhu, M. C.; Huang, Y. Y.; Ma, J. P.; Hu, S. M.; Wang, Y.; Guo, J.; Zhao, Y. X.; Wang, L. S. Coordination polymers based on organic-inorganic hybrid rigid rod comprising a backbone of Anderson-Evans POMs. *Cryst. Growth Des.* **2019**, *19*, 925−931. (b) Gao, N.; Du, Z.; Guan, Y. J.; Dong, K.; Ren, J. S.; Qu, X. G. Chirality-selected chemical modulation of amyloid aggregation. *J. Am. Chem. Soc.* **2019**, *141*, 6915−6921. (c) Vanhaecht, S.; Quanten, T.; Parac-Vogt, T. N. A simple nucleophilic substitution as a versatile postfunctionalization method for the coupling of nucleaophiles to an Anderson-type polyoxometalate. *Inorg. Chem.* **2017**, *56*, 3095−3101.
(28) (a) Wilson, E. F.; Miras, H. N.; Rosnes, M. H.; Cronin, L. Real-time observation of self-assembly of hybrid polyoxometalates using mass spectrometry. *Angew. Chem., Int. Ed.* **2011**, *50*, 3720−3724. (b) Surman, A. J.; Robbins, P. J.; Ujma, J.; Zheng, Q.; Barran, P. E.; Cronin, L. Sizing and discovery of nanosized polyoxometalate clusters by mass spectrometry. *J. Am. Chem. Soc.* **2016**, *138*, 3824−3830. (c) Thiel, J.; Yang, D. M.; Rosnes, M. H.; Liu, X. L.; Yvon, C.; Kelly, S. E.; Song, Y. F.; Long, D. L.; Cronin, L. Observing the hierarchical self- assembly and architectrural bistability of hybrid molecular metal oxides using ion-mobility mass spectraometry. *Angew. Chem., Int. Ed.* **2011**, *50*, 8871−8875.
(29) Yu, B.; Zou, B.; Hu, C. W. Recent applications of polyoxometalates in CO_2 capture and transformation. *J. CO_2 Util.* **2018**, *26*, 314−322.
(30) (a) Huang, K.; Zhang, J. Y.; Liu, F. J.; Dai, S. Synthesis of porous polymeric catalysts for the conversion of carbon dioxide. *ACS Catal.* **2018**, *8*, 9079−9102. (b) Yang, Q.; Yang, C. C.; Lin, C. H.; Jiang, H. L. Metal-organic-frmework-derived hollow N-doped porous carbon with ultrahigh concentrations of single Zn atoms for efficient carbon dioxide conversion. *Angew. Chem., Int. Ed.* **2019**, *58*, 3511−3515. (c) Liu, Y. X.; Wang, H. H.; Zhao, T. J.; Zhang, B.; Su, H.; Xue, Z. H.; Li, X. H.; Chen, J. S. Schottky barrier induced coupled interface of electron-rich N-doped carbon and electron-deficient Cu: In-built lewis acid-base pairs for highly efficient CO_2 fixation. *J. Am. Chem. Soc.* **2019**, *141*, 38−41. (d) He, L.; Nath, J. K.; Lin, Q. P. Robust multivariate metal-porphyrin frameworks for efficient ambient fixation of CO_2 to cyclic carbonates. *Chem. Commun.* **2019**, *55*, 412−415.
(31) (a) Lu, J. K.; Ma, X. Y.; Singh, V.; Zhang, Y. J.; Wang, P.; Feng, J. W.; Ma, P. T.; Niu, J. Y.; Wang, J. P. Facile CO_2 cycloaddition to epoxides by using a tetracarbonyl metal selenotungstate derivate $[\{Mn(CO)_3\}_4(Se_2W_{11}O_{43})]^{8-}$. *Inorg. Chem.* **2018**, *57*, 14632−14643. (b) Cheng, W. W.; Xue, Y. S.; Luo, X. M.; Xu, Y. A rare three-dimensional POM-based inorganic metal polymer bonded by CO_2 with high catalytic performance for CO_2 cycloaddition. *Chem. Commun.* **2018**, *54*, 12808−12811. (c) Jia, J. M.; Niu, Y. J.; Zhang, P. P.; Zhang, D. D.; Ma, P. T.; Zhang, C.; Niu, J. Y.; Wang, J. P. A monomeric tricobalt(II)-substituted Dawson-type polyoxometalate decorated by a metal carbonyl group: $[P_2W_{15}O_{56}Co_3(H_2O)_3(OH)_3Mn(CO)_3]^{8-}$. *Inorg. Chem.* **2017**, *56*, 10131−10134. (d) Ge, W. L.; Wang, X. C.; Zhang, L. Y.; Du, L.; Zhou, Y.; Wang, J. Fully-occupied Keggin type polyoxometalate as solid base for catalyzing CO_2 cycloaddition and Knoevenagel condensation. *Catal. Sci. Technol.* **2016**, *6*, 460−467.
(32) Sheldrick, G. M. Crystal structure refinement with SHELXL. *Acta Crystallogr., Sect. C: Struct. Chem.* **2015**, *C71*, 3−8.
(33) Nomiya, K.; Takahashi, T.; Shirai, T.; Miwa, M. Anderson-type heteropolyanions of molybdenum (VI) and tungsten (VI). *Polyhedron* **1987**, *6*, 213−218.

https://dx.doi.org/10.1021/acs.inorgchem.1c00019
Inorg. Chem. 2021, 60, 3980−3987